Clayton, C. R. I., Xu, M. & Bloodworth, A. (2006). *Géotechnique* **56**, No. 8, 561–571

A laboratory study of the development of earth pressure behind integral bridge abutments

C. R. I. CLAYTON*, M. XU† and A. BLOODWORTH*

A conventional bridge abutment utilises bearings to support the bridge deck, and expansion joints to allow it to slide as temperature changes occur. But experience has shown that expansion joints often leak, leading to deterioration of underlying structural elements, and are expensive to maintain and replace. As a result integral abutments, which are fully fixed with respect to the bridge deck, are increasingly being recommended. However, there is uncertainty about the magnitude of the earth pressures that they should be required to support. Available evidence from model tests and from field instrumentation does not provide a basis upon which to predict either the circumstances under which thermal cycling will lead to significant increases in earth pressure, or the levels to which they might rise. This paper reports the result of laboratory tests on natural clay samples, on pluviated sand specimens, and on glass ballotini, all of which have been subjected to the stress paths and levels of cyclic straining that a typical integral bridge abutment might impose on its retained soil. The results show that whereas the natural clay and the glass ballotini showed no lateral stress accumulation, regardless of strain levels and stress excursions, the pluviated sand specimens experienced systematic increases in lateral stress for almost all cyclic strain levels, eventually reaching states of stress at, or close to, both active and passive. The underlying mechanisms of stress increase are explored, and it is concluded that particle shape is an important factor in determining the response of soil to this special type of loading.

KEYWORDS: clays; laboratory tests; repeated loading; sands; stiffness; stress paths

Un contrefort de pont conventionnel utilise des appuis pour soutenir le tablier de pont et des joints de dilatation pour donner à la structure une flexibilité de glissement en fonction des changements de température. Cependant l'expérience montre que ces joints sont souvent sujets aux fuites et provoquent une détérioration des éléments structurels sous-jacents. Ils sont en outre coûteux en terme de maintenance et remplacement. C'est pourquoi les contreforts à culées intégrées, qui sont parfaitement fixes relativement au tablier du pont, sont de plus en plus recommandés. Il subsiste cependant une incertitude concernant la magnitude des pressions terrestres auxquelles il leur est demandé de résister. Les informations disponibles à ce sujet, fournies par des tests de modèles et une instrumentation in situ, ne forment pas une base suffisante pour prédire les circonstances dans lesquelles le cycle thermique conduira à des augmentations significatives de la pression terrestre ou les niveaux que celles-ci pourraient atteindre. Cet article présentent les résultats de tests obtenus en laboratoire, réalisés sur des échantillons d'argile naturels, sur des spécimens déposés par la méthode pluviale et sur des microsphères de verre. Tous ces échantillons ont été soumis aux cheminements de contraintes et aux niveaux de déformation cyclique qui pourraient être imposés à la masse de sol retenue pour un pont équipé de contreforts à culées intégrées typique. Les résultats obtenus indiquent que, si les échantillons d'argile naturelle et les microsphères de verre ne montrent aucune accumulation de contrainte latérale, quels que soient le niveau de contrainte appliqué et les plages de contraintes, les spécimens déposés par la méthode pluviale affichent une augmentation systématique de la contrainte latérale pour pratiquement tous les niveaux de contrainte cyclique, atteignant finalement des états de contrainte qui sont actifs et passifs, ou proches de l'être. Les mécanismes sous-jacents d'augmentation de la contrainte sont ici explorés et mènent à conclure que la forme des particules constitue un facteur important pour déterminer le comportement du sol en réponse à ce type de charge spécifique.

INTRODUCTION

A simple road bridge conventionally consists of a deck resting on an abutment at each of its ends. Because of daily and seasonal temperature variation, the deck expands and contracts longitudinally. However, the supporting abutments are relatively insensitive to changes in air temperature, and remain spatially fixed. To accommodate the relative movement, and prevent temperature-induced stresses from developing between superstructure and abutments, expansion joints and bearings have historically been installed between the deck and the abutments.

Over the past 30 years engineers have become increasingly aware of the disadvantages associated with the use of expansion joints and bearings. They have a relatively short life, failing as a result of penetration of deicing salts (Wallbank, 1989), or because of the accumulation of debris in the expansion space. They are expensive to purchase, install, maintain, and repair, and replacement inevitably causes disruption of traffic (Biddle *et al.*, 1997). Failure to maintain or replace expansion joints and bearings will lead to increased longitudinal deck loading, with possible overstressing and damage occurring to weaker bridge components (Biddle *et al.*, 1997).

Because of an increasing awareness of the problems associated with joints and bearings, there has been a return

Manuscript received 1 April 2005; revised manuscript accepted 1 August 2006.
Discussion on this paper closes on 2 April 2007, for further details see p.ii.
* School of Civil Engineering and the Environment, University of Southampton, UK.
† MacDonald, formerly School of Civil Engineering and the Environment, University of Southampton, UK.

to the concept of physically and structurally connecting the superstructure and abutments (Hambly, 1997), to create what is referred to as an *integral bridge*. An integral bridge eliminates the cost of the provision of movement joints and bearings, simplifies the construction process (Biddle *et al.*, 1997), avoids maintenance costs, and provides greater earthquake resistance. It is for these reasons that this form of structure has been widely adopted in the USA (Nicholson, 1997). In the UK, integral bridges have been encouraged over the past decade, especially by the publication of BD 57/95 (Highways Agency, 1995). However, concerns have remained about the levels of lateral stress that may be imposed on integral abutments. Despite considerable research, uncertainties still exist.

BACKGROUND

Because of their integral connection with the superstructure, integral bridge abutments attempt to move away from the soil they retain when the temperature decreases and the deck contracts (e.g. in the winter, and at night), and towards the soil when the temperature rises and the deck expands (e.g. in the summer, and during the daytime). As a consequence, the soil retained by the abutment is subjected to temperature-induced cyclic loading.

Research into the magnitude of earth pressures behind integral bridge abutments has to date taken three forms: field monitoring of full-scale structures (Broms & Ingleson, 1971, 1972; Hoppe *et al.*, 1996; Darley *et al.*, 1996, 1998; Barker & Carder, 2000, 2001); model tests, either in the centrifuge or under normal gravity (Springman *et al.*, 1996; England *et al.*, 2000; Goh, 2001; Cosgrove & Lehane, 2003; Tapper & Lehane, 2004); and numerical modelling (Springman *et al.*, 1996; Wood & Nash, 2000).

Despite the large number of integral bridge abutments that have been constructed in the USA, the design of this type of bridge appears to have been somewhat empirical (Nicholson, 1997). Shallow bank-seat piled abutments and shallow bank-seat spread-footing abutments are preferred in the USA, and the small height of such abutments limits the load that they can exert on the deck (Biddle *et al.*, 1997). In the UK bank seats are less popular, with full-height abutments being relatively common. The changes in earth pressure, and therefore the loads that can be exerted as a result of deck expansion and contraction, are potentially much larger.

Pressure changes observed during monitoring and model testing of cyclic wall movements have fallen into two groups: reversible pressure changes, and progressive changes in pressure with increasing numbers of loading cycles. Field monitoring and model testing programmes have in the past treated the integral abutment as a system comprising both the abutment and its retained soil, and have not sought to isolate or explain observations of pressure accumulation reported by, for example, Broms & Ingleson (1971), Moore (1985), Hoppe *et al.* (1996), and Cosgrove & Lehane (2003). This paper explores the behaviour of soil under the special type of cyclic loading that occurs behind a bridge abutment.

DEVELOPMENT OF LABORATORY TESTING METHODOLOGY

The laboratory testing reported in this paper was carried out to investigate the behaviour of soil subjected to the stress paths and strain levels that might be expected as a result of temperature increases on full-height integral bridge abutments. For the purposes of this investigation, it was considered that such abutments were likely to be constructed in two ways

(*a*) as diaphragm or bored pile walls, typically retaining overconsolidated clay (here termed an 'embedded' abutment)
(*b*) as backfilled walls, typically retaining compacted selected granular fill (here termed a 'frame' abutment).

Therefore two types of material were tested: 'undisturbed' clay and pluviated sand.

Materials tested

Tests were carried out on wireline rotary cored 'undisturbed' specimens of heavily overconsolidated Atherfield Clay taken from the Channel Tunnel Rail Link cut-and-cover tunnel site at Ashford, Kent, UK, and on pluviated specimens of Leighton Buzzard sand and glass ballotini. Electron micrographs of these three materials are shown in Fig. 1. It can be seen that whereas the ballotini (Fig. 1(a)) have a high degree of sphericity, the Leighton Buzzard sand (Fig. 1(b)), is sub-rounded, and somewhat irregular in shape. The Atherfield Clay (Fig. 1(c)) is platy, and appears to exhibit some anisotropy of structure shown by the preferential alignment of clay particles in the direction marked on the photomicrograph.

At Ashford the Atherfield Clay is stiff to very stiff and closely fissured. Samples were obtained of Atherfield I Clay, which forms the lower part of the deposit. It is chocolate brown, about 4·5 m thick at this location, and has a plasticity index of 20–30%. Its particle size distribution is shown in Fig. 2. The moisture contents and Atterberg limit values for the three specimens tested are given in Table 1.

Analysis of strains during isotropic consolidation and effective stress paths during monotonic shearing suggested (Graham & Houlsby, 1983) that the stiffness of the Atherfield I Clay was strongly anisotropic, with an effective Young's modulus in the horizontal direction of between 1·6 and 2·1 times that in the vertical direction, depending upon the specimen and method used to estimate it.

The Leighton Buzzard B sand is a light-brown sub-rounded, uniform, natural, uncrushed silica sand. It is free from silt, clay or organic matter and has a particle size between 0·6 mm and 1·18 mm (Fig. 2). It is extracted from part of the Lower Greensand at Leighton Buzzard, Bedfordshire, UK. The sand used in this research was supplied by David Ball Group plc of Cambridge, UK. The glass ballotini had a similar grading (Fig. 2) and were made from high-quality and pure soda-lime glass. They were supplied by Jencons Ltd of Leighton Buzzard, UK.

Test method

In order to provide a simplified loading scheme for laboratory triaxial stress path testing, five factors were considered

(*a*) the size of the idealised abutment and position of a representative soil element
(*b*) the starting stresses to be imposed on the element, representing those resulting from the weight of overburden, installation of the wall, and backfilling
(*c*) the stress path that would be imposed on the representative element as a result of abutment movements
(*d*) the magnitude of strain cycles that would be imposed by a typical range of temperature change and of deck lengths
(*e*) the initial direction of loading.

These matters are considered below.

A typical full-height abutment for a basic grade-separated

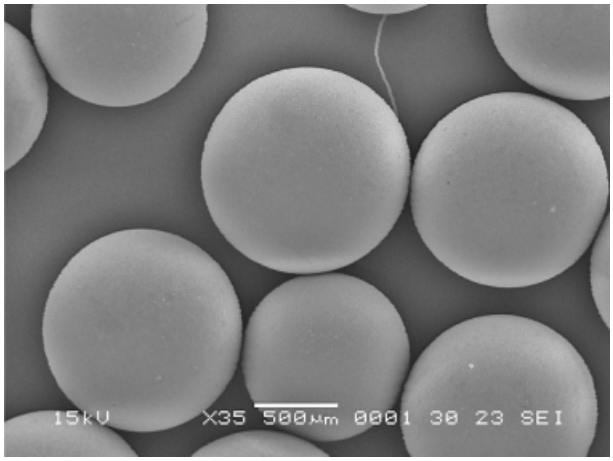

×20 (approx.) magnification
(a)

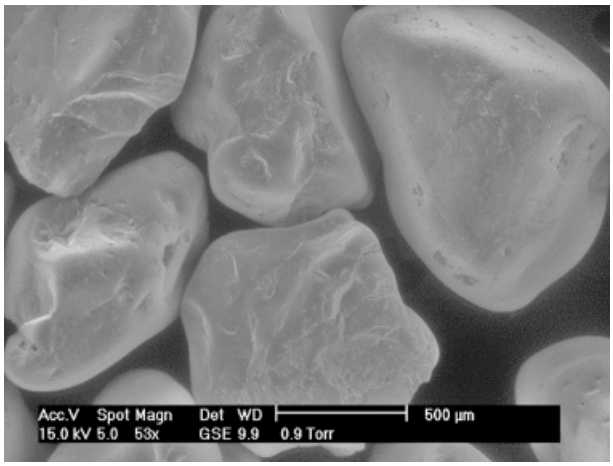

×30 (approx.) magnification
(b)

Possible preferential alignment of clay particles

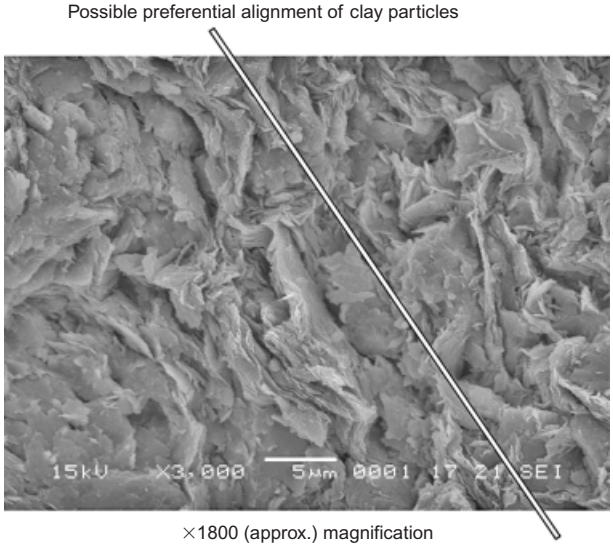

×1800 (approx.) magnification
(c)

Fig. 1. Scanning electron micrographs: (a) glass ballotini; (b) Leighton Buzzard B particles; (c) Atherfield I Clay

highway intersection will stand about 8 m above the lower road level. A *representative soil element* (Fig. 3(a)) was taken to be at mid-height, that is, at a depth of 4 m below the top of the bridge deck, and at a small distance behind the abutment wall. Although changes in earth pressure coefficient may not (depending on the mode of wall movement)

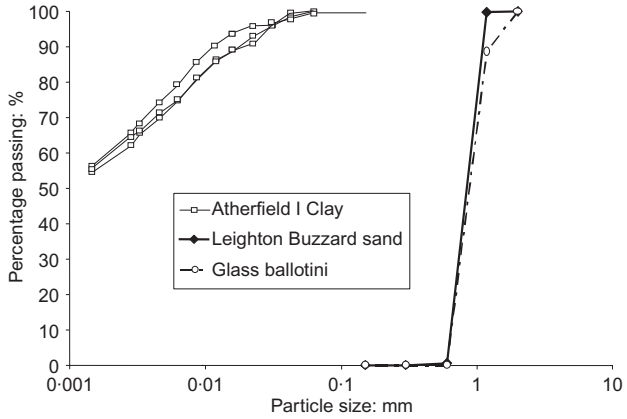

Fig. 2. Particle size distributions of Atherfield I Clay, Leighton Buzzard sand and glass ballotini

be as large at this level as near the surface of the backfill, the backfill is subjected to greater vertical stress levels, and the lateral stress changes induced will have a greater effect on the bending moments in a propped wall.

The *initial stresses* following abutment construction were estimated on the basis of installation effects (for bored pile or diaphragm wall abutments) and compaction pressures (for backfilled abutments). For stiff clay, the lateral earth pressure coefficient can be expected to drop approximately to unity, mainly because of the effect of wall installation (Clayton & Symons, 1992). Further decreases may occur because of excavation in front of the wall, but the magnitude is difficult to predict because it depends on the detailed construction sequence and technique. To take account of these uncertainties, different initial stress states were applied to the clay specimens before cyclic loading. Details can be found in Xu (2005).

Although granular material is usually compacted in thin layers behind a frame bridge abutment, Clayton & Symons (1992) have demonstrated that the depth to which compaction pressures are significant will not exceed 3–4 m, below which the horizontal earth pressure coefficient can reasonably be assumed to equal K_0 for relatively rigid walls such as abutments. For sand, the representative soil element was therefore considered to be below the depth affected by compaction pressures, and (with one exception) the first cyclic loading started from the earth pressure at rest (K_0) state, with $\sigma'_v = 80$ kPa.

For simplicity the abutment wall was assumed to be smooth, because this avoids the need to introduce principal stress rotations during cycling. For a smooth abutment wall the thermal movements of the deck essentially lead to changes in the horizontal total stress between the wall and the soil, while the vertical total stress in the soil remains constant, fixed by the weight of overburden. The intermediate stress will depend upon the geometry of the abutment and transverse restraint that it applies to the soil. For simplicity the tests described in this paper were conducted in the triaxial apparatus, with the *total stress path* fixed (Fig. 3) regardless of the imposed strains.

The strain imposed on a representative soil element can, for a relatively stiff abutment wall rotating about its base (the case of a frame abutment), be estimated from the displacement induced at the top of the abutment (δ) by the thermal movement of the deck. For a retained fill of height H the horizontal strain is approximately δ/H (Bransby, 1972; Bolton & Powrie, 1988; Lehane, 1999). If rotation occurs at some greater depth (as in the case of an embedded abutment) then strains near the top of the abutment wall will be proportionately lower.

Table 1. Summary of undrained testing on Atherfield I Clay specimens

Specimen	m/c, PL, LL: %	p'_0: kPa	Test description
AC1	20, 23, 44	360	Triaxial compression to failure
AC2	20, 22, 44	80	Radial cyclic loading at 0·04% (5 cycles) and 0·075% (3 cycles)
		80	Radial extension to failure
AC3	19, 22, 46	76	Radial cyclic loading at 0·025% (6 cycles), 0·05% (6 cycles), 0·1% (4 cycles) and 0·15% (1 cycle)
		76	Drained cycling (not reported here)
		115	Radial extension and compression at 0·05%
		230	Triaxial compression to failure

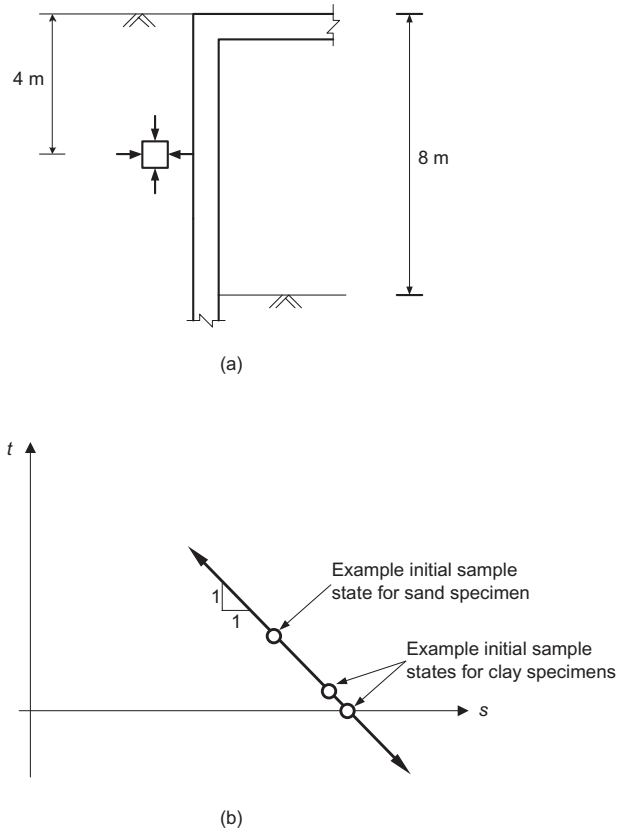

Fig. 3. (a) Location of representative soil element; (b) example total stress path for constant vertical total stress

For example, a concrete-decked integral bridge constructed in the London area can be expected to experience an annual change in effective bridge temperature (EBT) of 43°C, resulting in a change in deck length of 0·52 mm/m length (Emerson, 1976). According to the simplified method above, and provided the temperature changes result in equal displacements at each abutment, a 60 m long deck retaining 8 m of soil and subjected to an EBT change of 43°C will impose a horizontal strain of 0·2% on the soil behind its integral abutments. Shorter decks, taller abutments and smaller temperature changes will produce proportionately smaller strains. Finite element analyses carried out by Springman *et al.* (1996), by Lehane (1999), and for the geometry adopted in this paper by the authors, suggest that, for the range of stiffness to be expected, the soil behind the abutments provides little restraint to the deck, and that the horizontal strain levels predicted by simple methods are of the correct order of magnitude.

It is clearly possible that a bridge deck and abutment backfilling might be completed in either the summer or the winter months. However, Springman *et al.* (1996) have demonstrated that the *initial direction of loading* has no influence on sand behaviour during subsequent cyclic loading.

APPARATUS AND TEST PROGRAMME

Element testing was carried out in a Bishop and Wesley apparatus (Bishop & Wesley, 1975). The specimens were 100 mm in diameter and approximately 200 mm high. Local axial strain was measured using two submersible LVDTs, and radial strain was measured at specimen mid-height using a caliper (Bishop & Henkel, 1962), modified to accept a submersible LVDT, and in sand with an internal plate to avoid membrane penetration and thinning (Bica, 1991). For clay specimens, mid-plane pore pressure measurement was carried out using a flushable probe with a high-air-entry stone (Sodha, 1974).

The Atherfield Clay specimens were initially subjected to stepped increases in cell pressure, during which time pore pressures were carefully monitored. Once the B value reached 0·97 a back-pressure equal to the mid-plane pore pressure was applied, and the specimens were swelled to an isotropic effective stress level of approximately 80 kPa, equivalent to that of a soil element at a depth of 4 m with groundwater at 3 m below the surface. Following a rest period, which depended on the loading excursion size and was typically about 1 day at the radial strain level of 0·1%, the specimens were cycled undrained under strain control along the total stress path shown in Fig. 3. Cyclic radial strains of between 0·01% and 0·15% were applied in the various tests. Most tests began with a reduction in horizontal stress, simulating the abutment moving away from the soil. However, for the radial strain range of 0·04% on AC2, the soil was first subjected to 0·02% radial compression, which was then followed by 0·04% radial strain extension and cycling. The initial direction of loading did not appear to influence the results obtained from the test.

For specimen AC2, cyclic deformation was followed by undrained monotonic compressive loading until an axial strain of 2·4% was reached. The test on specimen AC3 consisted of four stages. First, undrained radial-strain-controlled cyclic testing was performed. This was followed by drained radial-strain-controlled cyclic testing, which will not be reported here. In the third stage, the specimen was consolidated to an isotropic initial mean effective stress of 115 kPa, after which undrained loading was carried out to a radial strain of 0·05%. Finally, the specimen was consolidated to an isotropic initial mean effective stress of 230 kPa, after which the specimen was sheared undrained to failure under a constant cell pressure.

Initial testing of the granular material was designed to investigate the influence of initial sand density and cyclic radial strain range on the behaviour of granular materials behind typical frame integral abutments. It consisted of three sand specimens (LBS1, LBS2 and LBS3; Table 2), each

Table 2. Test programmes on coarse Leighton Buzzard sand and glass ballotini specimens

Specimen	Density	Dry density: Mg/m^3	Voids ratio, e	D_r: %	K_0	Cyclic radial strain ranges: %	Number of cycles
LBS1	Loose	1·54	0·72	18	0·5	0·05	120
						0·1	170
						0·2	60
LBS2	Dense	1·67	0·59	70	0·42	0·05	60
						0·1	50
						0·2	30
LBS3	Very dense	1·73	0·53	93	0·32	0·05	54
						0·1	250
LBS4	Loose	1·54	0·72	18	0·5	0·006*	50
						0·012†	100
						0·012‡	50
G1	Dense	1·61	0·553	76	0·47	0·05	15

*Stage 1: between active and isotropic state.
†Stage 2: only across isotropic state.
‡Stage 3: only touching the active state.

with a different density, on which different cyclic radial strain ranges were applied. Specimens of both Leighton Buzzard sand and glass ballotini were formed by pluviation through a funnel, under water (Bishop & Eldin, 1950).

Normally, it can be expected that the granular material behind a frame integral abutment will be in a dense condition, as a result of compaction. However, loose granular backfill has also been considered, as a possible means of avoiding high earth lateral pressures (Card & Carder, 1993). Therefore, in addition to the very dense and medium dense sand specimens, a loose sand specimen was also tested in the experimental programme.

Drained K_0 loading was initially carried out on each specimen in order to reach the desired initial vertical effective stress of 80 kPa. This was followed by drained strain-controlled cyclic loading (to 0·05%, 0·1% and 0·2% strain), with a machine (external) strain rate of 6% per day. On each specimen, the smallest cyclic strain excursions were applied first. It was assumed that the first temperature changes would result in deck expansion, and all cycling therefore began with a horizontal stress increase (i.e. stresses moving towards the passive failure state).

Further tests were carried out in order to investigate the source of lateral stress accumulation that had been observed in tests LBS1, LBS2 and LBS3. During these tests all specimens had approached active failure and undergone a 90° principal stress rotation in every cycle of loading. To investigate the influence of the active state and the principal stress reversal separately, test LBS4 (Table 2) was carried out. Cycling of test specimen LBS4 under 0·006% radial strain, which neither crossed the isotropic state nor approached the active state, was stopped when stable behaviour was observed. The horizontal stress was then increased, taking the specimen along the stress path shown in Fig. 3 until a deviatoric stress of −30kPa was obtained. Radial-strain-controlled cyclic loading was then re-applied, but with an increased strain range of 0·012%. This took the specimen across the isotropic stress line, causing a 90° rotation of the major principal stress, but without reaching the active state. Strains again stabilised, and the specimen was then loaded to the active state along the same stress path. Radial-strain-controlled cyclic loading was then performed without reaching the isotropic stress state and subjecting the specimen to 90° principal stress rotation. The cyclic radial strain range for this stage was 0·012%.

To investigate the hypothesis that stress build-up might be associated with particle shape, a dense glass ballotini specimen was tested (Table 2, Test G1). The initial test procedure was the same as for test LBS1. Strain-controlled cyclic stress path loading was applied under a cyclic radial strain range of 0·05%.

RESULTS AND DISCUSSION

Tests on Atherfield Clay

Figure 4 shows vertical undrained secant Young's modulus curves as a function of local axial strain for two specimens of Atherfield Clay (AC1 and AC3) loaded vertically, in an undrained triaxial compression test. Also shown are the equivalent curves, but at lower effective stress levels, for Atherfield Clay specimens swelled back to the mean effective stress of the representative element, and then loaded horizontally, changing the radial total stress while holding the vertical total stress constant. For these curves the horizontal undrained secant Young's modulus is plotted as a function of the horizontal (radial) strain. The rate of stiffness reduction with increasing axial strain is similar for the two types of loading. As shown in the inset to the figure, the initial portions of the stress paths are not vertical in q/p' stress space, suggesting anisotropy of stiffness (Graham & Houlsby, 1983).

Although the very small strain stiffness (G_{max}) of soils is best normalised with regard to $p'^{0·5}$, previous studies (Jardine *et al.*, 1991) have suggested that, at the intermediate strains relevant to this work, stiffness of clay can be normalised by p'_0. Differences between the curves are shown after normalising the data by the initial mean effective stress (p'_0) at the start of shearing in Fig. 5. The two specimens loaded radially display higher normalised stiffnesses at very small strain levels, but differences are small at intermediate strains. When normalised by $p'^{0·5}_0$ the vertical undrained Young's moduli for the triaxial compression tests are consistently higher than the horizontal Young's moduli for the radially loaded specimens.

Figure 6 shows curves of deviator stress as a function of radial strain for Atherfield Clay specimen AC2 under undrained cyclic loading with constant vertical total stress. For clarity, only the first and last cycles of loading under each level of cyclic strain are presented. Each cycle consisted of four phases:

(*a*) decrease of horizontal total stress at a rate of 2% radial strain per day
(*b*) rest period at constant strain, until the rate of change of

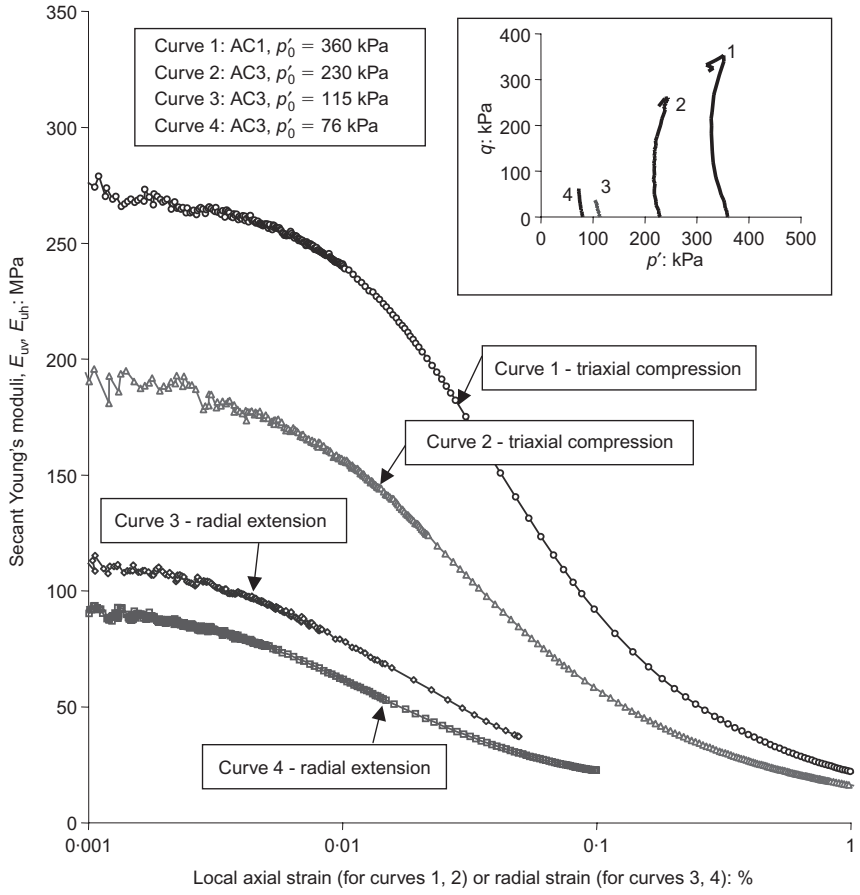

Fig. 4. Variation of undrained secant Young's modulus as function of local strain for two specimens loaded in triaxial compression and two specimens loaded horizontally

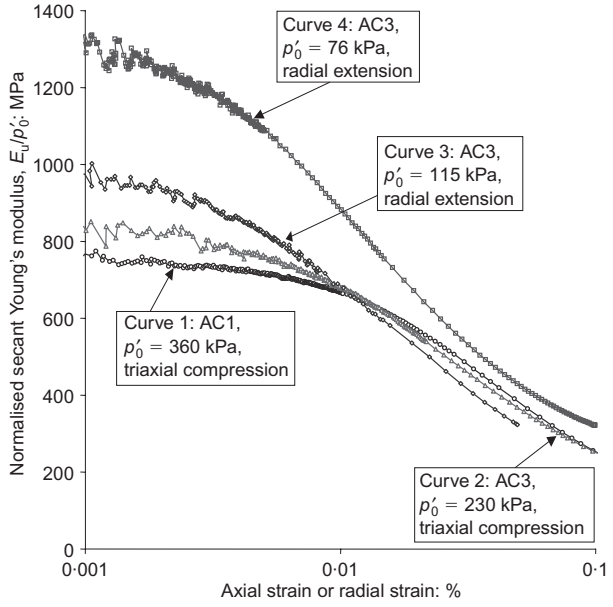

Fig. 5. Comparison of undrained secant Young's moduli after normalisation for specimens loaded axially and radially

deviator stress decreased to less than 0·36 kPa/h, which was approximately 1/100th of the initial rate of change of deviator stress in each cycle

(*c*) increase of horizontal total stress at a rate of 2% radial strain per day

(*d*) rest period under constant strain, until the rate of change of stress decreased to less than 0·36 kPa/h.

As the vertical stress was held constant during cycling loading under strain control, increases in horizontal stress are associated with reductions in the deviator stress q in Fig. 6. It can be seen that each strain excursion leads to a change of horizontal stress, which is reduced to some extent by creep during the rest period. The strain rates imposed on the clay were considerably greater than those to be expected behind a bridge abutment, which might be of the order (at most) of only 0·1% per day. Under slower loading it might be expected that most of the excess lateral pressure, subsequently lost during the rest periods, would not occur. In an additional test carried out 10 times more slowly the horizontal stress returned to the same post-creep end point as for the faster test shown in Fig. 6, but the maximum horizontal stress was reduced.

As can be seen in the example given in Fig. 6, there was very little change in lateral pressure as a result of cycling. Most of this occurred during the first cycle. For specimen AC2 the total increase in radial stress over the entire cycling phase was 3·4 kPa (or 7·7%), whereas for Specimen AC3 it was 4·1 kPa (7·4%).

The small-strain stiffnesses observed during each cycle of loading were not significantly affected either by previous cycles at the same strain level or by previous cycling at smaller strain levels. Fig. 7 shows stiffness degradation curves for cyclic strain levels of 0·05%, 0·1% and 0·15%. For all practical purposes the curves are identical, except towards the end of the cycle, where some stiffening appears to occur, perhaps as a result of previous loadings to this strain level, coupled with creep during the rest periods. The

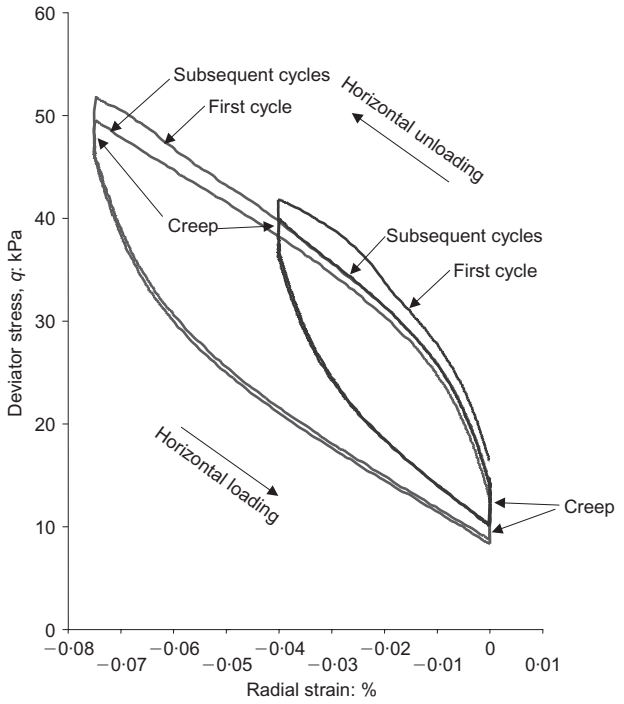

Fig. 6. Deviator stress as a function of radial strain for Atherfield Clay specimen AC2

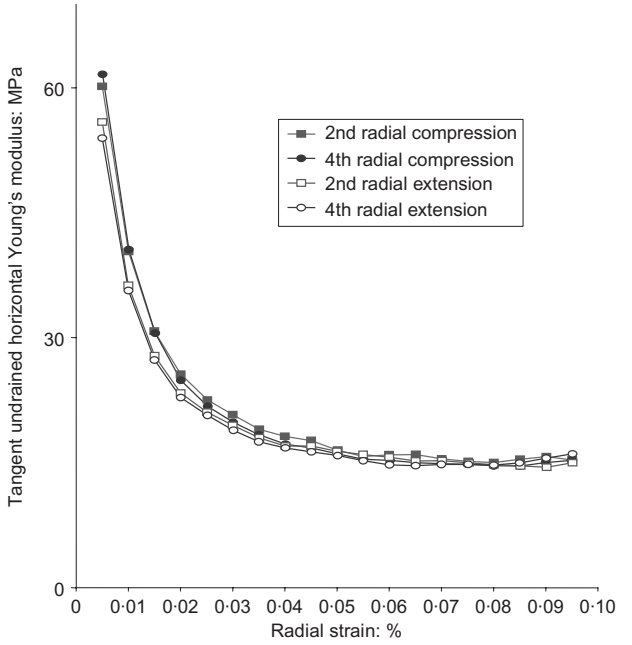

Fig. 8. Comparison of stiffness degradation in two cycles of loading. Radial strain range 0·1%, specimen AC3

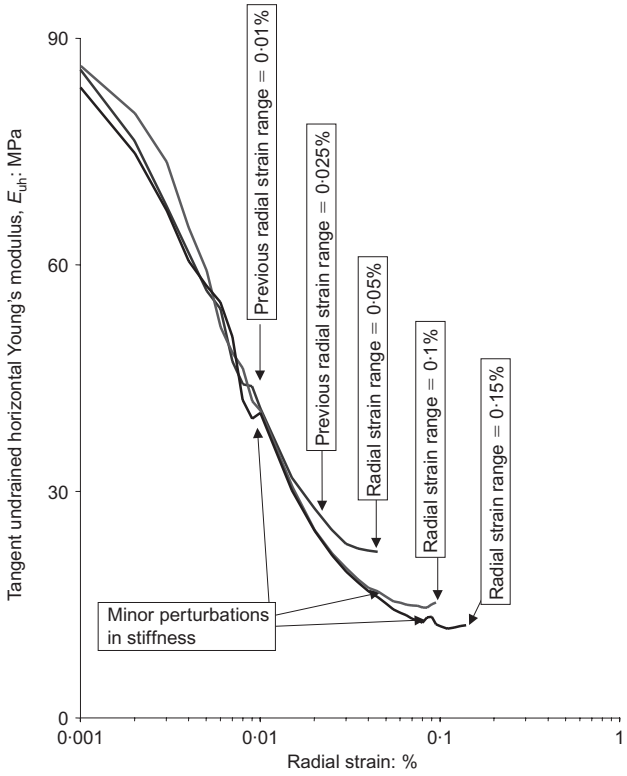

Fig. 7. Effect of repeated loading to increasing strains on stiffness degradation during loading towards radial extension. Specimen AC3, last loadings at given strain ranges

maximum previous strain level appears to produce a minor perturbation in the current tangent stiffness curve. Fig. 8 compares the tangent-stiffness against strain behaviour for horizontal loading and unloading. The similarity between the curves results partly from the fact that the mean effective stress remained more or less constant during undrained loading, but may also be because strains during loading and unloading of this heavily overconsolidated clay are likely to have resulted from particle bending, rather than rolling, sliding or crushing. Although stiffness during horizontal loading was somewhat larger than during unloading, once again the differences were small.

Tests on granular material

Table 2 provides a summary of the test programmes carried out on the Leighton Buzzard sand and the glass ballotini. As a result of the higher stiffness of the Leighton Buzzard sand when compared with that of the Atherfield Clay, much larger horizontal stress changes were observed when applying the first cycle of horizontal loading to the sand. Fig. 9 shows deviator stress and earth pressure coefficient K ($= \sigma'_h/\sigma'_v$) as a function of local radial strain for the loose sand specimen LBS1 under a cyclic radial strain range of 0·05%. It will be recalled that the specimen was brought to its starting vertical effective stress of 80 kPa under K_0 conditions. From the early stages of cycling the specimen approached active failure conditions (recall that $K_a = 0{\cdot}3$ for $\phi' = 32°$, approximately the critical state angle of friction) during radial strain decrease. There was a progressive increase in maximum lateral pressure, and at the same time the density of the specimen increased. As can be seen from Fig. 9, after 100 cycles under a radial strain of 0·05% the stresses during cycling showed no signs of stabilising, and the minimum deviator stress ($q = (\sigma_a - \sigma_r)$) had reached about -50 kPa, equivalent (for fully drained conditions) to a horizontal total stress of 130 kPa in a fully drained granular backfill.

Figure 10 shows that, in contrast to the behaviour of the Atherfield Clay, the loose Leighton Buzzard sand had markedly different stiffness when loading and unloading in the horizontal direction. Furthermore, these evolved during cycling, with both the stiffnesses during horizontal loading and unloading increasing very significantly. Given that the strains applied to the soil are controlled by the expansion of the bridge deck, an increase in stiffness leads to an increase in the stress excursion in the backfill. Once the minimum

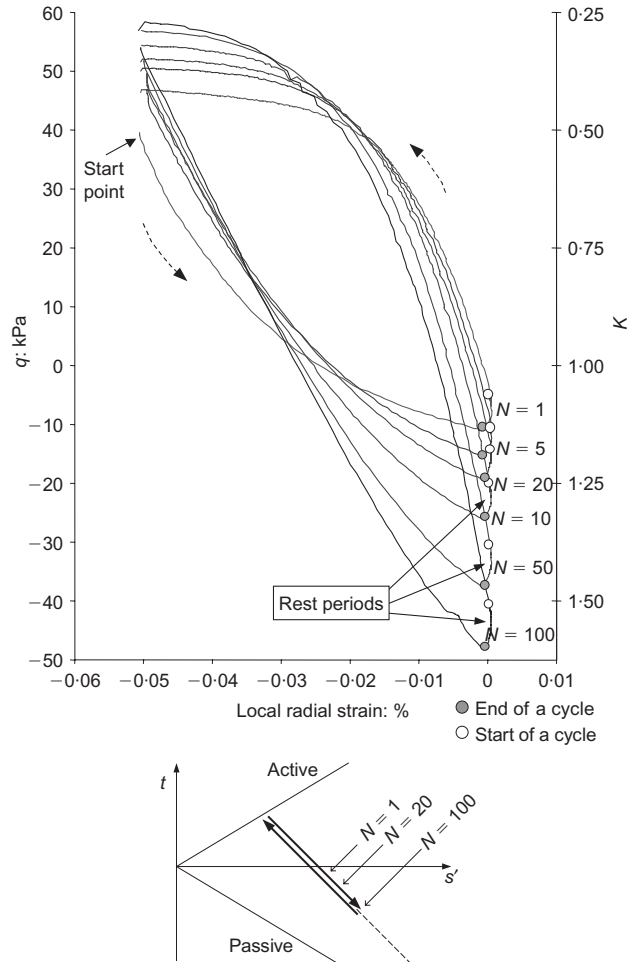

Fig. 9. Deviator stress and earth pressure coefficient K as a function of local radial strain for loose sand specimen LBS1 under a cyclic radial strain range of 0·05%

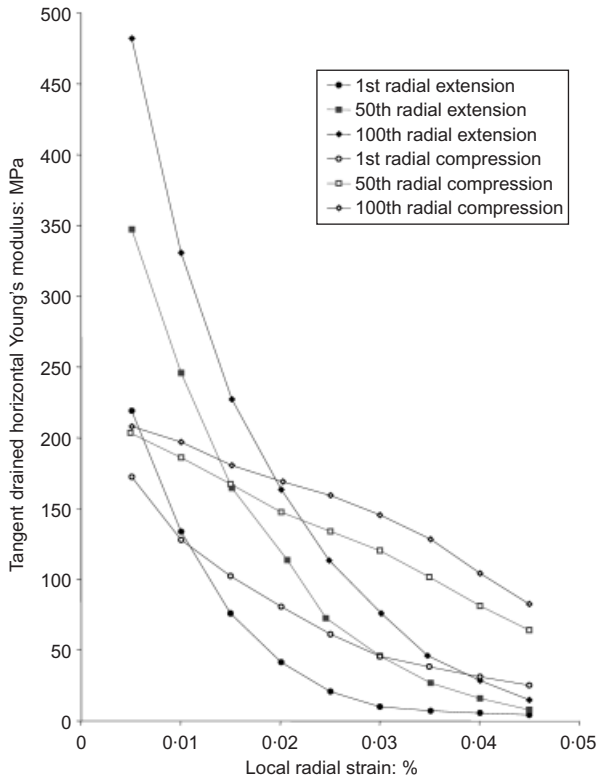

Fig. 10. Stiffness of specimen LBS1 under cyclic loading, as a function of local radial strain

pressure is constrained by the limiting active value, cycling necessarily leads to increases in the maximum lateral stress if the soil stiffness increases.

Various mechanisms and causes of continuing horizontal stress increase during cycling have been postulated. For example:

(*a*) evolution of stiffness, perhaps associated with increases in the density of the sand during cyclic loading
(*b*) differences in stiffness during radial loading and unloading, perhaps due to 90° principal stress rotations when crossing the mean stress axis, or due to particle rotations when approaching active conditions.

Data were re-examined, and further experiments carried out in order to search for controlling factors.

Test LBS1 had been carried out on a loose specimen, with a relative density of only 18% (Table 2), and significant volumetric compression (5%) had been measured under cycling, during which time the relative density had risen by almost 30%. Test LBS2 was then carried out on a dense specimen ($D_r = 70\%$), and once again significant increases in lateral stress were observed as a result of cycling. A very dense specimen (LBS3, $D_r = 93\%$) was then tested under horizontal strain ranges of 0·05% and 0·1%. After small initial volumetric and axial strain compressions in the first 20 cycles at 0·1% strain, the density of the specimen decreased systematically, reaching a relative density of slightly above 90% after a total of 300 cycles. During this time, the maximum coefficient of earth pressure rose to about 5. These results strongly suggested that the mechanism leading to progressive horizontal stress increase during thermal cycling was not associated with densification of the backfill.

It has already been seen (compare Fig. 8 and Fig. 10) that the stiffness of granular material under constant vertical effective stress cycling is more complex than that of natural overconsolidated clay. It seems probable that such behaviour is at least partly attributable to changes in packing and loading arrangements of the particles, which it was thought might be associated with principal stress rotation and failure. To test these hypotheses, additional tests were carried out on Leighton Buzzard sand specimen LBS4, shown diagrammatically in Fig. 11.

In contrast with the results of the tests on loose specimen LBS1, no progressive increase in horizontal stress was observed during Stage 1 of the test on loose specimen LBS4, when it was cycled between the active and the isotropic states. The same behaviour was observed in Stage 2, where a 90° principal stress rotation was applied to the specimen. However, in Stage 3, where the stress path approached active failure but did not cross the isotropic stress state, there was a progressive increase in horizontal stress until the experiment was stopped after 50 cycles (Fig. 12). The volumetric strain change was approximately equal in each of the three stages of the test, again supporting the finding that the evolution of maximum horizontal stress is not necessarily associated with volumetric strain.

It is clear from recent work (Clayton *et al.*, 2004; Wesseloo, 2004) on gold tailings that particle shape, and in particular sphericity, has a significant effect on the behaviour of granular materials. Fig. 1(b) shows that the Leighton Buzzard sand, although rounded, is not completely spherical. The observations in the tests on specimen LBS4 had suggested that the progressive increase of maximum horizontal stress during cycling was associated with the active state, and therefore (e.g. Skinner, 1969) with rotation of particles. A test was therefore carried out on a glass ballotini bead

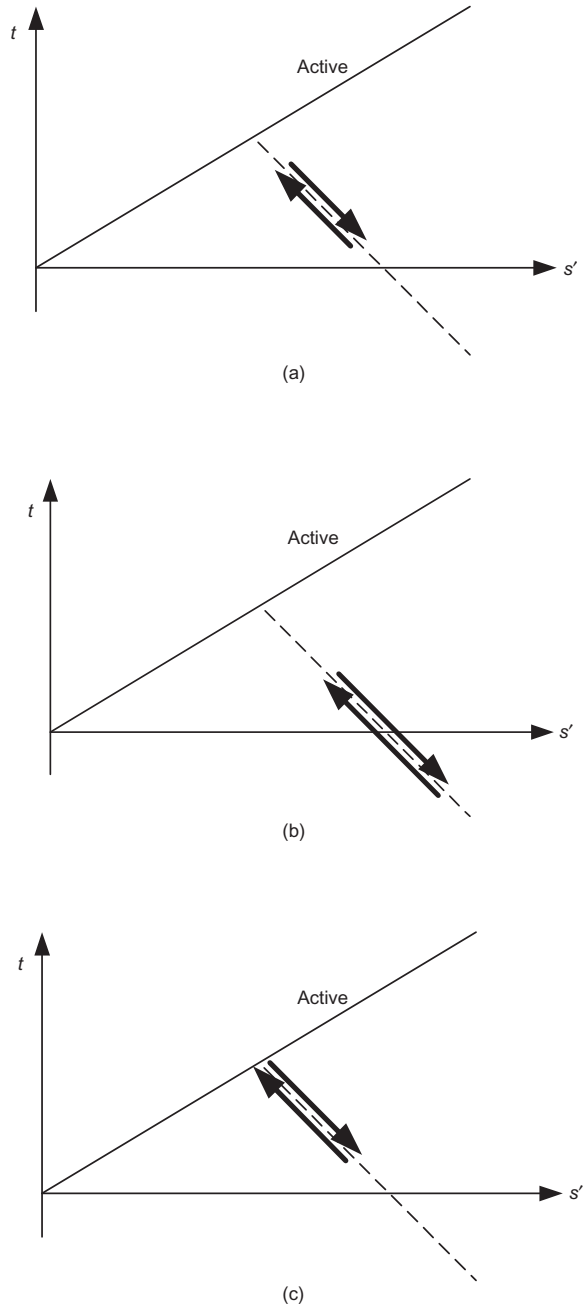

Fig. 11. Stages of test LBS4: (a) stage 1, cycling between the active state and the isotropic state; (b) stage 2, cycling across the isotropic stress state; (c) stage 3: cycling reaching the active state

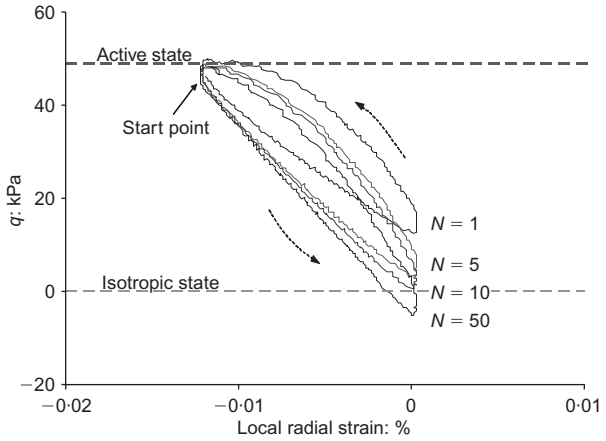

Fig. 12. Deviator stress against radial strain during test LBS4 on loose sand during Stage 3 (begun from the active state, but above the isotropic state; cyclic radial strain range = 0·012%)

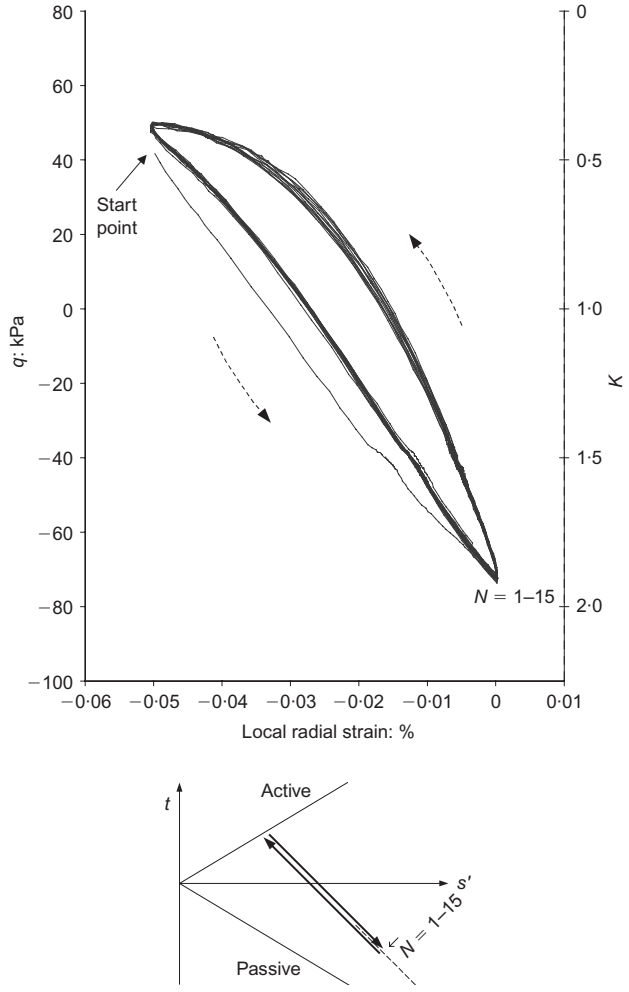

Fig. 13. Deviator stress against local radial strain for the dense glass ballotini under a cyclic radial strain range of 0·05% (15 cycles)

(Fig. 1(a)), with the expectation that there would be less evolution of stress resulting from a more spherical material. Fig. 13 shows the variations of deviator stress as a function of local radial strain for dense glass ballotini under 15 cycles with a radial strain range of 0·05%. The material behaviour stabilises after the first cycle, with no increase in either the minimum or the maximum horizontal stress being apparent. Tangent drained horizontal Young's moduli are plotted against linear strain level in Fig. 14(a). They show a rapid stiffness decrease upon radial unloading, fairly constant stiffness during radial loading, and no evolution of stiffness with cycling. Normalisation removes the effect of current mean effective stress and, as shown in Fig. 14(b), gives a picture of quite uniform stiffness behaviour during cycling. The tangent stiffness of loose Leighton Buzzard sand during radial extension, normalised with respect to current mean stress (p'), is compared with that of the glass ballotini in Fig. 15. The continuing evolution of the stiffness of the sand is in contrast to the relatively constant stiffness of the ballotini.

Figure 16 shows that for the loose Leighton Buzzard sand specimen (LBS1; $D_r = 18\%$) the maximum effective earth pressure coefficient ($K_{max} = (\sigma'_h/\sigma'_v)_{max}$) reached a value of

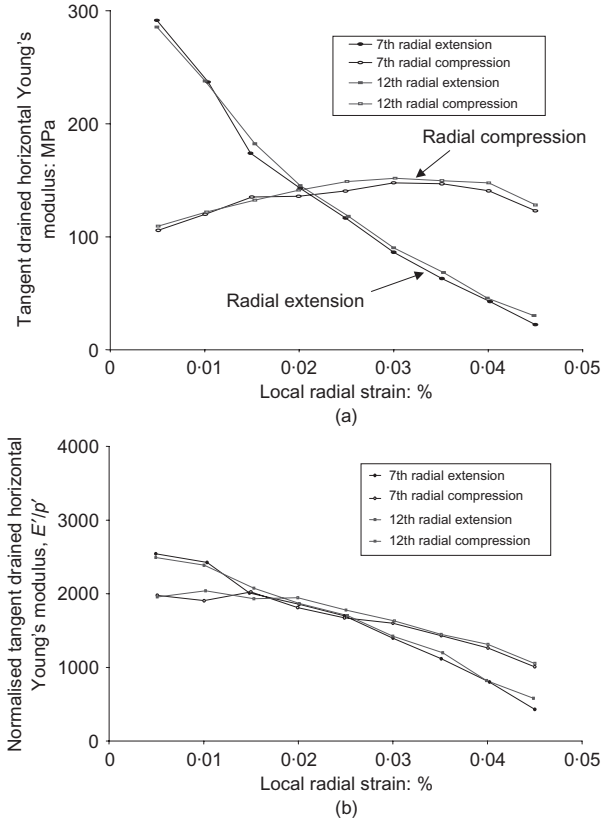

Fig. 14. Stiffness of glass ballotini under cyclic loading, as a function of local radial strain.

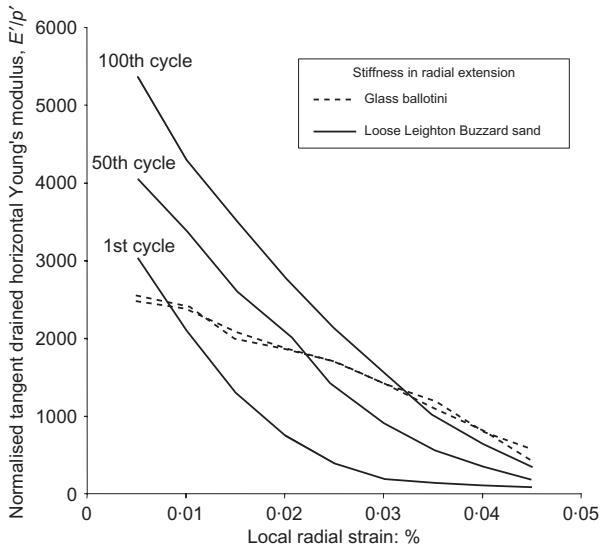

Fig. 15. Comparison of normalised tangent stiffness of loose Leighton Buzzard sand and glass ballotini

almost 3 after almost 350 cycles with a maximum radial strain range of 0·2%. Tests on the dense Leighton Buzzard sand (LBS2; $D_r = 70\%$) showed a more rapid rise in maximum earth pressure coefficient, with K_{max} rising to almost 3 after only 130 cycles with a maximum radial strain range of 0·2%. In the test on very dense Leighton Buzzard sand, K_{max} reached almost 5 after 300 cycles with a maximum radial strain range of only 0·1% strain. For this specimen, subsequent loading to failure under triaxial compression gave $\phi' = 43°$, equivalent to a Rankine passive

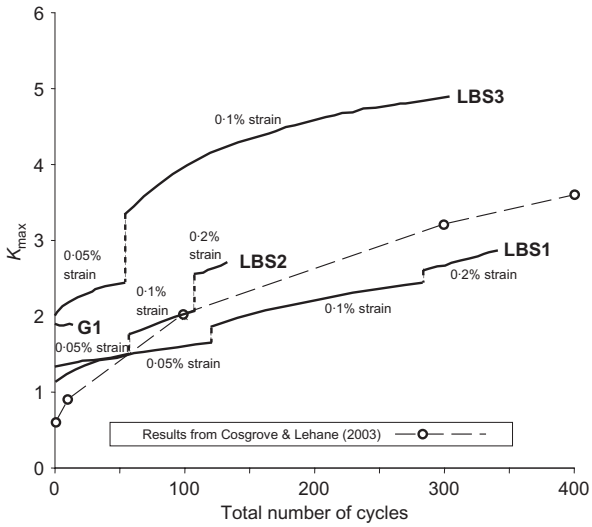

Fig. 16. Maximum earth pressure coefficients (K_{max}) against total number of cycles for Leighton Buzzard sand specimens

earth pressure coefficient of 5·3. As can be seen from Fig. 16, maximum earth pressures continued to rise at the end of all the tests. Data from Cosgrove *et al.* (2001), who recorded a stress accumulation under vertical cyclic testing on a fine sand specimen, although for a much larger strain magnitude, are shown in Fig. 16 for comparison.

CONCLUSIONS

Strain-controlled stress path triaxial tests have been carried out on undisturbed cohesive soil specimens, and on pluviated granular materials using stress paths and strain levels similar to those to be expected in a soil element at mid height behind a full-height abutment.

The results of triaxial testing show, over the range of horizontal strains that might be expected in the field, that significant diurnal and seasonal horizontal stress changes can be expected behind integral bridge abutments. The magnitude of these stress changes will depend largely upon the horizontal stiffness of the backfill or soil. For the Atherfield Clay, undrained stiffness during cyclic horizontal loading was shown to be strain level dependent, but did not vary significantly from compression to extension, or change with increasing number of cycles.

Build-up of maximum horizontal stress with horizontal strain cycling has been observed for specimens of Leighton Buzzard sand over a wide range of density. The test results reported here suggest that it is associated with irregular but relatively rotund particle shape, and that it is not the result of densification during cycling. Cosgrove *et al.* (2001) have suggested that this is the result of structural or fabric changes; the results presented here indicate that it is associated with readjustment of particles close to, or at the, active stress state. Neither natural cohesive soil nor perfectly spherical glass ballotini showed significant signs of stress increase, even for the wide range of cyclic strain levels that were imposed.

Once stress increase was initiated, maximum stresses rose continuously, and moved towards the passive state. Further testing will be required to establish whether this effect is restricted to certain particle shapes and a uniform grading, or whether it is the norm for materials composed of relatively rotund particles.

The maximum earth pressure coefficients recorded at the end of each test on Leighton Buzzard sand were considerably higher than either active or at-rest values, and even

after several hundred cycles were continuing to increase. A maximum effective principal stress ratio of about 5 was observed in the test on very dense Leighton Buzzard sand, which is close to the Rankine passive earth pressure coefficient calculated on the basis of the effective angle of friction of the sand specimen in triaxial compression. These results will therefore be of some concern to designers of integral bridge abutments.

ACKNOWLEDGEMENTS

The work described in this paper was supported by the Engineering and Physical Sciences Research Council of the United Kingdom, by a PRC/Hong Kong Postgraduate Scholarship, and by an Overseas Research Studentship from Universities UK.

NOTATION

B	$\Delta u/\Delta\sigma_c$
D_r	relative density
e	voids ratio
H	retained height of soil or backfill
K	effective principal stress ratio, σ'_h/σ'_v
K_0	coefficient of earth pressure at rest
p, p'	mean total and effective stresses $= \frac{1}{3}(\sigma_v + 2\sigma_h)$ or $\frac{1}{3}(\sigma'_v + 2\sigma'_h)$
p'_0	mean effective stress at start of loading or unloading
q	principal stress difference in triaxial apparatus, $(\sigma_v - \sigma_h)$
s	$= \frac{1}{2}(\sigma_v + \sigma_h)$
s'	$= \frac{1}{2}(\sigma'_v + \sigma'_h)$
t	$= \frac{1}{2}(\sigma_v - \sigma_h)$
u	pore pressure
δ	displacement at top of abutment induced by changing temperature of deck
σ_a, σ'_a	axial total and effective stresses in triaxial apparatus
σ_c	cell pressure in triaxial apparatus
σ'_h	horizontal effective stress
σ_r, σ'_r	radial total and effective stresses in triaxial apparatus
σ'_v	vertical effective stress

REFERENCES

Barker, K. J. & Carder, D. R. (2000). *Performance of the two integral bridges forming the A62 Manchester Road Overbridge*, TRL Report 436. Crowthorne: Transport Research Laboratory.

Barker, K. J. & Carder, D. R. (2001). *Performance of an integral bridge over the M1–A1 Link Road at Bramham Crossroads*, TRL Report 521. Crowthorne: Transport Research Laboratory.

Bica, A. V. D. (1991). *A study of free embedded cantilever walls in granular soil*. PhD thesis, University of Surrey, Guildford.

Biddle, A. R., Iles, D. C. & Yandzio, E. D. (1997). *Integral steel bridges: Design guidance*, Publication No. P163. Ascot: Steel Construction Institute.

Bishop, A. W. & Eldin, G. (1950). Undrained triaxial tests on saturated sands and their significance in the general theory of shear strength. *Géotechnique* **2**, No. 1, 13–32.

Bishop, A. W. & Henkel, D. J. (1962). *The measurement of soil properties in the triaxial tests*, 2nd edn. London: Edward Arnold.

Bishop, A. W. & Wesley, L. D. (1975). A hydraulic triaxial apparatus for controlled stress path testing. *Géotechnique* **25**, No. 4, 657–670.

Bolton, M. D. & Powrie, W. (1988). Behaviour of diaphragm walls in clay prior to collapse. *Géotechnique* **38**, No. 2, 167–189.

Bransby, P. L. (1972). General theories of earth pressures and deformations. *Proc. 5th Eur. Conf. Soil Mech. Found. Engng, Madrid* **2**, 75–78.

Broms, B. B. & Ingleson, I. (1971). Earth pressure against the abutments of a rigid frame bridge. *Géotechnique* **21**, No. 1, 15–28.

Broms, B. B. & Ingleson, I. (1972). Lateral earth pressure on a bridge abutment. *Proc. 5th Eur. Conf. Soil Mech. Found. Engng, Madrid* **1**, 117–123.

Card, G. B. & Carder, D. R. (1993). *A literature review of the geotechnical aspects of integral bridge abutments*, TRL Project Report 52. Crowthorne: Transport Research Laboratory.

Clayton, C. R. I. & Symons, I. F. (1992). The pressure of compacted fill on retaining walls. *Géotechnique* **42**, No. 1, 127–130.

Clayton, C. R. I., Theron, M. & Vermeulen, N. J. (2004). The effect of particle shape on the behaviour of gold tailings. Advances in Geotechnical engineering: The Skempton Conference, Vol. 1, pp. 393–404. London: Thomas Telford.

Cosgrove, E. F. & Lehane, B. H. (2003). Cyclic loading of loose backfill placed adjacent to integral bridge abutments. *Int. J. Phys. Modelling Geotech.* **3**, No. 3, 9–16.

Cosgrove, E., Lehane, B. M. & Ng, C. W. W. (2001). Sand tested under cyclic triaxial conditions with constant radial stress. *Proc. 15th Int. Conf. Soil Mech. Found. Engng*, Istanbul, **1**, 63–66.

Darley, P., Carder, D. R. & Alderman, G. H. (1996). *Seasonal thermal effects on the shallow abutment of an integral bridge in Glasgow*, TRL Report 178. Crowthorne: Transport Research Laboratory.

Darley, P., Carder, D. R. & Barker, K. J. (1998). *Seasonal thermal effects over three years on the shallow abutment of an integral bridge in Glasgow*, TRL Report 344. Crowthorne: Transport Research Laboratory.

Emerson, M. (1976). *Bridge temperatures estimated from the shade temperature*, TRRL Report LR696. Crowthorne: Transport Research Laboratory.

England, G. L., Tsang, C. M. & Bush, D. (2000). *Integral bridges – a fundamental approach to the time temperature loading problem*. London: Thomas Telford.

Goh, D. (2001). *The behaviour of shallow abutments of integral bridges*. PhD thesis, University of Birmingham.

Graham, J. & Houlsby, G. T. (1983). Elastic anisotropy of a natural clay. *Géotechnique* **33**, No. 2, 165–180

Hambly, E. C. (1997). Integral bridges. *Proc. Inst. Civil Engnrs—Transport Engineering* **123**, No. 1, 30–38.

Highways Agency (1995). *BD 57 Design for durability*, DMRB 1·3. London: HMSO.

Hoppe, E. J. & Gomez, J. P. (1996). *Field study of an integral backwall bridge*, Virginia Transportation Research Council Final Report. Charlottesville, VA: Transportation Research Council.

Jardine, R. J., Potts, D. M., St John, H. D. & Hight, D. W. (1991). Some practical applications of a non-linear ground model. *Proc. 10th Eur. Conf. Soil Mech. Found. Engng, Florence* **1**, 223–228.

Lehane, B. M. (1999). Predicting the restraint provided to integral bridge deck expansion. *Proc. 12th Eur. Conf. Soil Mech. Geotech. Engng, Amsterdam* **2**, 797–802.

Moore, S. R. (1985). *Earth pressure on spill-through abutments*. PhD thesis, University of Surrey.

Nicholson, B. A. (1997). *Integral bridges: Report of a study tour to North America*. Crowthorne: Concrete Bridge Development Group.

Skinner, A. (1969). A note on the influence of interparticle friction on the shearing strength of a random assembly of spherical particles. *Géotechnique* **19**, No. 1, 150–157.

Sodha, V. (1974). *The stability of embankment dam fills of plastic clays*. MPhil thesis, Imperial College, University of London.

Springman, S. M., Norrish, A. & Ng, C. W. W. (1996). *Cyclic loading of sand behind integral bridge abutments*, Transport Research Laboratory Project Report 146. Crowthorne: Transport Research Laboratory.

Tapper, L. & Lehane, B. M. (2004). Lateral stress development on integral bridge abutments. *Proc. 18th Australasian Conf. Mech. Struct. Mat.*, Perth, **2**, pp. 1069–1076.

Wallbank, J. (1989). *The performance of concrete in bridges: A survey of 200 highway bridges*. London: HMSO.

Wesseloo, J. (2004). *The strength and stiffness of geocell support packs*. PhD thesis, University of Pretoria, South Africa.

Wood, D. M. & Nash, D. (2000). Earth pressures on an integral bridge abutment: a numerical case study. *Soils Found.* **40**, No. 6, 23–38.

Xu, M. (2005). *The behaviour of soil behind full-height integral abutments*. PhD thesis, University of Southampton.